Energies **2013**, *6*, 492-513; doi:10.3390/en6010492

OPEN ACCESS

energies

ISSN 1996-1073

www.mdpi.com/journal/energies

Article

Gas Path Health Monitoring for a Turbofan Engine Based on a Nonlinear Filtering Approach

Feng Lu [1,2,*], Jinquan Huang [1,*] and Yiqiu Lv [1]

[1] College of Energy and Power Engineering, Nanjing University of Aeronautics and Astronautics, Nanjing 210016, China; E-Mail: lyqnuaa@126.com

[2] Aviation Motor Control System Institute, Aviation Industry Corporation of China, Wuxi 214063, China

* Authors to whom correspondence should be addressed; E-Mails: lfaann@nuaa.edu.cn (F.L.); jhuang@nuaa.edu.cn (J.H.); Tel.: +86-139-5162-8575 (F.L.).

Received: 21 September 2012; in revised form: 4 December 2012 / Accepted: 27 December 2012 / Published: 17 January 2013

Abstract: Different approaches for gas path performance estimation of dynamic systems are commonly used, the most common being the variants of the Kalman filter. The extended Kalman filter (EKF) method is a popular approach for nonlinear systems which combines the traditional Kalman filtering and linearization techniques to effectively deal with weakly nonlinear and non-Gaussian problems. Its mathematical formulation is based on the assumption that the probability density function (PDF) of the state vector can be approximated to be Gaussian. Recent investigations have focused on the particle filter (PF) based on Monte Carlo sampling algorithms for tackling strong nonlinear and non-Gaussian models. Considering the aircraft engine is a complicated machine, operating under a harsh environment, and polluted by complex noises, the PF might be an available way to monitor gas path health for aircraft engines. Up to this point in time a number of Kalman filtering approaches have been used for aircraft turbofan engine gas path health estimation, but the particle filters have not been used for this purpose and a systematic comparison has not been published. This paper presents gas path health monitoring based on the PF and the constrained extend Kalman particle filter (cEKPF), and then compares the estimation accuracy and computational effort of these filters to the EKF for aircraft engine performance estimation under rapid faults and general deterioration. Finally, the effects of the constraint mechanism and particle number on the cEKPF are discussed. We show in this paper that the cEKPF outperforms the EKF, PF and EKPF, and conclude that the cEKPF is the best choice for turbofan engine health monitoring.

Keywords: turbofan engine; performance estimation; nonlinear filter; extended Kalman filter; particle filter

1. Introduction

Gas turbine engines are highly complex systems consisting of static and rotating components, along with associated subsystems, controls, and accessories. They are required to provide reliable power generation over thousands of flight cycles while being subjected to a broad range of operating loads and conditions, including extreme temperature environments [1]. Performance and reliability of aircraft turbofan engines gradually deteriorate over their service life due to degradation of the gas path components such as fan, compressor, combustor, and turbines [2]. Common causes of degradation of the gas path components include compressor fouling, increase of the blade-tip clearance in the turbine, labyrinth seal leakage, wear and erosion, and corrosion in the hot sections. Foreign-object damage, caused by impingement of such foreign objects as birds, pieces of ice, and runway debris, will rapidly affect the component performance [3,4]. These physical faults lead to degradation of the health parameters, such as thermodynamic efficiency and flow capacity of individual gas-path components. Performance degradation, in turn, causes changes in the observable parameters, such as temperature, pressure, rotational speed, and fuel flow rate. Gas path health monitoring plays a critical role in improving safety, reliability, availability, and affordability. The cost-saving potential of such health evaluations is substantial, but only if the performance estimation are reliable [5,6].

Several approaches have been introduced to estimate the performance of gas turbine engines. Luppold proposed using a Kalman filter to estimate in-flight engine performance variations [7]. Doel presented an assessment of weighted-least-squares-based gas path analyses [8]. Depold applied expert systems and neural networks to gas turbine prognostics and diagnostics [9]. Joly discussed gas-turbine diagnostics using artificial neural-networks for a high bypass ratio military turbofan engine [10]. Kobayashi proposed a hybrid neural network-genetic algorithm technique for aircraft engine performance diagnostics [11]. Ogaji reported a fuzzy logic approach for gas turbine fault diagnostics [12]. Volponi compared the use of Kalman filter and neural network methodologies in gas turbine performance diagnostics [13]. Dimogianoppoulos discussed aircraft engine health estimation via stochastic modeling of flight data interrelations [14]. Li reported a novel nonlinear weighted-least-squares method, combined with the fault-case concept and the GPA index for effective gas-turbine fault detection, isolation and quantification [15–17].

Compared to the data-based approaches, such as the neural network and fuzzy logic, the Kalman filter approach utilizes all model information available, can deal with the fact faults may not be known, and offers better estimation accuracy. Therefore, the variants of the Kalman filter are widely used for gas path analysis of gas turbine engines. Brotherton presented an approach that fused a physical model called self tuning on-board real-time model (STORM) with an empirical neural net model to provide a unique hybrid model called enhanced STORM (eSTORM) for engine diagnostics based on the Kalman filter [18]. Volponi developed eSTORM, and provided a means to automatically tune for the engine model to a particular configuration as the engine evolved over the course of its life, furthermore,

aligned the model to the particular engine being monitored to insure accurate performance tracking, while not compromising real-time operation [19]. Simon D. applied constrained Kalman filtering, along with constraint tuning on the basis of measurement residuals, to estimate engine health parameters [20,21]. Litt proposed a real-time Kalman filter approach for estimation of helicopter engine degradation due to compressor erosion [22]. Simon D.L. developed a systematic sensor selection approach and an optimal tuner selection approach for on-board self-tuning engine models, respectively [23,24]. Kobayashi reported application of a constant gain extended Kalman filter for in-flight estimation of aircraft engine health parameters [25], and a baseline system based on Kalman filter for aircraft engine on-line diagnostics [26]. Borguet presented adaptive filters to track gradual deterioration and rapid deterioration [27]. Naderi proposed a nonlinear multiple model fault detection and isolation scheme for health monitoring of jet engines [28].

The piecewise-linear dynamic scheduled models, from the component-level model of gas turbine engine, are required for gas path health monitoring via linear a Kalman filter in the flight envelope, and linearization errors that decrease the accuracy of performance estimation are inevitable. The EKF method is often used for state estimation with the assumption of weak nonlinear Gaussian systems [29] in the references above, and the performance depends on how often Jacobians are updated. In practice the turbofan engine is a complex system with strong nonlinear and non-Gaussian noise. Recently, a popular solution strategy, sequential Monte Carlo sampling based particle filters, has been successfully used for the nonlinear and non-Gaussian state estimation problems, since it does not necessitate simplification of nonlinearity or any assumption of specific distributions [30–34]. Orchard presented the implementation of a particle-filtering-based framework for calculating the probability of blade cracking and the remaining useful life in a turbine engine [35]. Li introduced the particle filter into the application of unmanned aerial vehicle (UAV) engine fault prediction [36], and then Gerasimos studied and compared nonlinear Kalman filtering methods and particle filtering methods for estimating the state vector of UAVs through the fusion of sensor measurements [37]. Gross compared the performance of three nonlinear estimators—the extended Kalman filter, the sigma-point Kalman filter, and the particle filter—for global positioning system/inertial navigation system (GPS/INS) sensor fusion for aircraft navigation systems approaches [38]. The EKF algorithm is used as the proposal distribution for PF importance sampling to avoid the particle degeneration in [39–41].

For the reasons described above, variants of the PF algorithm are used for the strong nonlinear and non-Gaussian systems. However, the PF has not been introduced to the problem of aircraft engine gas path performance estimation so far, which is usually strongly nonlinear and non-Gaussian. This paper presents the applications of turbofan engine gas path health monitoring based on particle filters, and gives a systematic comparison of the estimation accuracy and computational effort of various nonlinear filter based approaches to gas path performance estimation. Because the EKF requires a computational effort that is an order of magnitude lower than that of the UKF, the proposal distribution in the PF is calculated by the EKF in the paper. Considering the magnitude limitation of gas path degradation, the constrained extended Kalman filter particle filter is developed based upon the EKPF.

We emphasize that in this paper we are confining the problem to the turbofan engine health estimation in the presence of performance abrupt shifts and the gradual degradation with the cycle number. The performance estimation systems with Gaussian noise, non-Gaussian noise process noise are built up, and simulation results show that the constrained EKPF method enhances the robustness of

PF algorithm against poor prior information. The comparisons of the EKPF and the cEKPF on estimate accuracy with the less measurement numbers are carried out, and validate that the estimate capability of the cEKPF outperforms that of the EKPF. The experiments and analysis show that compared to the known filtering approaches for aircraft engine gas path monitoring, the proposed cEKPF has better efficiency and is more compliant to the problem of health estimates with constraints.

This paper is organized as follows: Section 2 discusses the formulation of different nonlinear filtering approaches containing the EKF, the PF, and the constrained EKPF. Section 3 details the problem of turbofan health parameter estimation, along with the dynamic model that we use in our simulation experiments. Section 4 shows some simulation results based on a nonlinear turbofan model. We see in this section the comparison of the nonlinear filtering approaches with the respect in the accuracy and the computational effort. Section 5 presents some concluding remarks and suggestions for further work.

2. State Estimation for Nonlinear Systems

In this section we first review the extension of the standard Kalman filter to nonlinear systems: the extend Kalman filter. Then we discuss the sequential Monte Carlo sampling algorithm known as the PF, and present the constrained EKPF.

2.1. The Extended Kalman Filter

Consider the discrete nonlinear time-invariant system represented by the following form:

$$\begin{aligned} x_{aug,k+1} &= \begin{pmatrix} x_{k+1} \\ h_{k+1} \end{pmatrix} = f(x_k, h_k, u_k) + w_k \\ y_k &= h(x_k, h_k, u_k) + v_k \end{aligned} \tag{1}$$

where k is the time index, x is the state vector, h is the performance vector, u is the know control input, y is the measurement, $\{w_k\}$ is the process noise sequences, $\{v_k\}$ is the measurement noise sequences, and x_{aug} is the augment state vector. The problem is to find an estimate $\hat{h}_{k+1}$ of h_{k+1} given the measurements $\{y_0, y_1, \cdots, y_k\}$. We assume that the following standard conditions are satisfied:

$$\begin{aligned} &E[x_0] = \bar{x}_0 \\ &E[w_k] = E[v_k] = 0 \\ &E\left[(x_0 - \bar{x}_0)(x_0 - \bar{x}_0)^T\right] = P_0^+ \\ &E\left[w_k w_m^k\right] = Q\delta_{km} \\ &E\left[v_k v_m^k\right] = R\delta_{km} \\ &E\left[w_k v_m^k\right] = 0 \end{aligned} \tag{2}$$

The EKF has a predictor-corrector structure and involves only basic linear algebra operations. This algorithm for the nonlinear system of Equation (1) starts with the time update equations:

$$\begin{aligned} P_k &= FP_{k-1}^{+}F^T + Q \\ \hat{x}_{aug,k} &= f\left(\hat{x}_{k-1}^{+}, \hat{h}_{k-1}^{+}, u_{k-1}\right) \end{aligned} \tag{3}$$

where the Jacobian in the preceding equation F is given as:

$$F = \frac{\partial f\left(\hat{x}_{k-1}^{+}, \hat{h}_{k-1}^{+}, u_{k-1}\right)}{\partial x} \tag{4}$$

Then the EKF performs the following measurement update equations:

$$\begin{aligned} K_k &= P_k H^T \left(HP_k H^T + R\right)^{-1} \\ \hat{x}_{aug,k}^{+} &= \hat{x}_{aug,k} + K_k\left[y_k - h\left(\hat{x}_{aug,k}\right)\right] \\ P_k^{+} &= \left(I - K_k H\right)P_k \end{aligned} \tag{5}$$

where the Jacobian in the measurement equation H is given as:

$$H = \frac{\partial h\left(\hat{x}_{aug,k}\right)}{\partial x} \tag{6}$$

Most of the computational effort is due to the system simulation that is required for nonlinear equation calculation, and the system simulations that are required to obtain the Jacobians F and H [42]. The estimation accuracy and computational effort of the EKF increase with the frequency of the Jacobian calculations. The Jacobian for the EKF is obtained by the relative perturbation approach, updated each step, and the requirements of real-time for gas path parameter estimation in the Component Level Model (CML) has been validated in previous research [29,46].

2.2. The Particle Filter

The EKF reviewed in Section 2.1 is the most widely applied state estimation algorithm for nonlinear systems. However, there are some disadvantages of EKF including: (i) the estimation may fail to converge to the true state if the system nonlinearities and non-Gaussianity are severe, and (ii) constraints are not considered in the algorithm.

For the turbofan engine and health monitoring model cases, Gaussianity both of the process noise or the measurement noise are no longer guaranteed, and thus approximate statistical solutions are needed. Particle filters are popular models for estimating the state of a dynamical nonlinear and non-Gaussian system become available on-line [30–32]. The algorithm generates a set of random samples, which is propagated and updated recursively to approximate the state probability density function (PDF) of the system.

Assume the prior distribution of the state of a dynamical system $p(x_0)$, and let $x_{0:k} \triangleq \{x_0, \cdots, x_k\}$ and $y_{1:k} \triangleq \{y_1, \cdots, y_k\}$ denote the series of state and measurement, respectively. It approximates any *a posteriori* PDF $p(x_{0:k} | y_{1:k})$ by a set of particles, $x_{0:k}^i$, and their associated weights, w_k^i, in a discrete summation form:

$$p(x_{0:k} \mid z_{1:k}) \approx \sum_{i=1}^{N} w_k^i \delta(x_{0:k} - x_{0:k}^i)$$
$$\sum_{i=1}^{N} w_k^i = 1, \qquad w_k^i \geq 0 \tag{7}$$

where N is the number of particles. The expect case for Monte Carlo sampling is to generate particles directly from the true posterior PDF $p(x_{0:k} \mid y_{1:k})$, which is generally unavailable. Thus we define the importance sampling distribution $q(x_{0:k} \mid y_{1:k})$ before sampling, and the weight w_k^i can be approximated as:

$$w_k^i \propto \frac{p(x_{0:k} \mid y_{1:k})}{q(x_{0:k} \mid y_{1:k})} \propto \frac{p(y_k \mid x_k^i) p(x_k^i \mid x_{k-1}^i) p(x_{0:k-1}^i \mid y_{1:k-1})}{q(x_k^i \mid x_{0:k-1}^i, y_{1:k}) q(x_{0:k-1}^i \mid y_{1:k-1})} = w_{k-1}^i \frac{p(y_k \mid x_k^i) p(x_k^i \mid x_{k-1}^i)}{q(x_k^i \mid x_{0:k-1}^i, y_{1:k})} \tag{8}$$

In the generic PF, the importance sampling distribution has the following equations:

$$q(x_k \mid x_{0:k-1}, z_{1:k}) = q(x_k \mid x_{k-1}, z_k)$$
$$q(x_k^i \mid x_{k-1}^i, z_k) = p(x_k^i \mid x_{k-1}^i) \tag{9}$$

With this choice and normalization, one can derive that the importance weights can be computed sequentially as:

$$w_k^i \propto w_{k-1}^i p(y_k \mid x_k^i)$$
$$w_k^i = w_k^i / \sum_{i=1}^{N} w_k^i \tag{10}$$

The generic PF algorithm has a significant drawback: after a certain number of recursive steps, all but one particle will have negligible weights w_k^i. This implies that a large computational effort which is devoted to updating particle is meaningless. Thus importance re-sampling is done assigning each particle with equal weight $w_k^i = 1/N$ whenever the effective number N_{eff} of particles becomes less than a threshold value N_{th}:

$$N_{eff} = \frac{1}{\sum_{i=1}^{N} \left(w_k^i\right)^2} < N_{th} \tag{11}$$

When N_{th} is close to value $N_{eff,k}$ then all particles have almost the same significance. The threshold value of N is usually taken as $N_{th} = \frac{2}{3} N$.

Estimation procedure of the PF algorithm is summarized as follows:

a. Prediction step:
   1. Initialization: Generate initial particles $\left\{x_0^i\right\}_{i=1}^{N}$ from a prior distribution $p(x_0)$;
   2. Importance sampling: Draw prior particles, $\left\{x_k^i\right\}_{i=1}^{N}$, from importance sampling distribution $p(x_k^i \mid x_{k-1}^i)$;

b. Update step:

3. Weighting: Evaluate the importance weights $w_k^i \propto w_{k-1}^i p(y_k \mid x_k^i)$ once new measurement is available, and normalize the weights $w_k^i = w_k^i / \sum_{i=1}^{N} w_k^i$;
4. Effective scale: Calculate effective particle set size N_{eff} with equation (11);
5. Resampling: Generate the posterior particles, $\{x_k^i\}_{i=1}^N$, based on their weights and resampling metric;
6. Output: Reset $w_k^i = 1/N$, and calculate the state estimate:

$$\hat{x}_k = \frac{\sum_{i=1}^{N} x_k^i}{N} \tag{12}$$

Set $k = k+1$ and go back to step (2).

2.3. The Constrained EKPF

Generic PF utilizes a sequential Monte Carlo method to approximate posterior distribution by using a set of weighted samples, therefore, it can theoretically represent any distribution. However, the proposal function of the particle filter algorithm is suboptimal, and it inevitably results in a particle degeneracy phenomenon. The main idea of EKPF algorithm is that the EKF is employed to approximate the mean and the covariance of the proposal distribution for each particle, rather than with the initial PDF for particles in the conventional PF algorithm. The EKPF is able to introduce the latest observation value to amend the state transition model of particles and its amount of calculation is quite small. The re-sampling process of the EKPF is similar to that of the PF. The particles in the EKPF fall into the overlap field of the prior and the likelihood as much as possible.

In the EKPF framework, the EKF approximates the optimal minimum-mean square error estimator of the system state by calculating the conditional mean of the state if given all of the observations. This is done in a recursive procedure by propagating the Gaussian approximation of the posterior distribution through time and combining it at each time step with the new observation. The posterior PDF is approximated at each time step as follows:

$$p\left(x_k \middle| y_k\right) \approx N\left(\hat{x}_k, \hat{P}\right) \tag{13}$$

where $\hat{x}_k$ is the estimated state, and $\hat{P}$ is the estimated covariance at time k from the measurement y_k. Each particle is updated by the EKF, and then it takes the approximated posterior PDF as importance sampling distribution:

$$q\left(x_k^i \middle| x_{k-1}^i, y_k\right) = N\left(\hat{x}_k^i, \hat{P}_k^i\right) \tag{14}$$

As shown in the conventional PF and the EKPF, it does not consider constraints. The nature of sample based representation of the PF facilitates incorporating constraints into the estimation procedure [43]. Gas path health parameters of turbofan engines vary within a certain range, therefore, the health parameter estimation is actually a state estimation problem with constraints. Kyriakides [44] and Lang [45] discuss how to accept/reject the particles in the PF based on constraint knowledge. The

disadvantage is that it discards all the particles violating constraints, reduces the number of various particles and may yield poor estimations.

An improved way to deal with constraints without completely discarding particles lying outside the constraint region is presented. A particle update mechanism used to handle constraints is developed in the EKPF framework. After the importance sampling by the EKF, each particle $x_k^i \in R^{l\times 1}$ is ascertained whether it is in the constraint region C:

$$x_k^i = \begin{cases} \left(x_k^i + x_{k-1}^i\right)/2 & x_k^i \in C \\ x_k^i & x_k^i \notin C \end{cases} \quad i = 1, \cdots, N \tag{15}$$

This process enables the algorithm to modify all the particles violating constraints. Each particle is an M-dimension vector, elements of which have constraints themselves. If the mth element of the modified particle $x_k^i(m)$ is still not in the corresponding range [$C_{min}(m)$, $C_{max}(m)$], then the boundary value is substituted for the value of the mth element and the other elements remain unchanged. The further adjustment expression is as follows:

$$x_k^i(m) = \begin{cases} C_{\max}(m) & x_k^i(m) > C_{\max}(m) \\ C_{\min}(m) & x_k^i(m) < C_{\min}(m) \\ x_k^i(m) & else \end{cases} \quad i = 1, \cdots, N \tag{16}$$

All particles will be reconstructed within the constraint region after being implemented by the update mechanism above, and then are used for state estimate next step. Estimation procedure of the constrained EKPF algorithm is detailed as shown in Figure 1; it mainly includes four steps: initialization, PDF calculation by the EKF, state update, and particles update with constraints.

Figure 1. Constrained EKPF algorithm procedure.

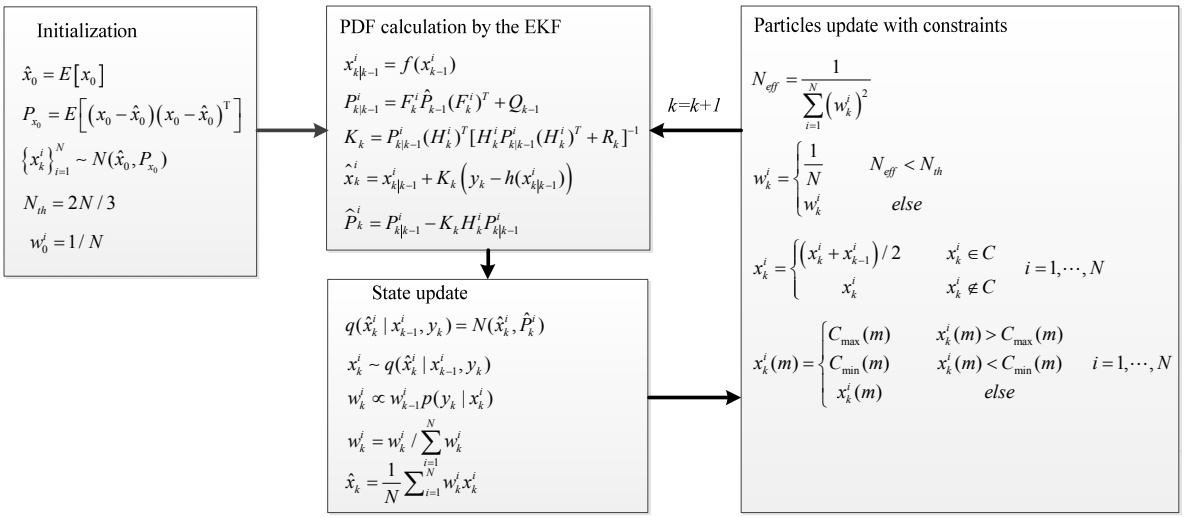

3. Turbofan Engine Gas Path Performance Estimation

The engine is a high bypass ratio turbofan engine, see Figure 2. A single inlet supplies airflow to the fan. Air leaving the fan separates into two streams: one stream passes through the engine core, and the other stream passes through the annular bypass duct and then leaves. The fan is driven by the low

pressure turbine. The air passing through the engine core moves through the compressor, which is driven by the high pressure turbine. Fuel is injected in the combustor and burned to produce hot gas for driving the turbines. The air leaves the low pressure turbine (LPT) through the nozzle, which has a variable cross section area.

Figure 2. Schematic representation of a turbofan engine.

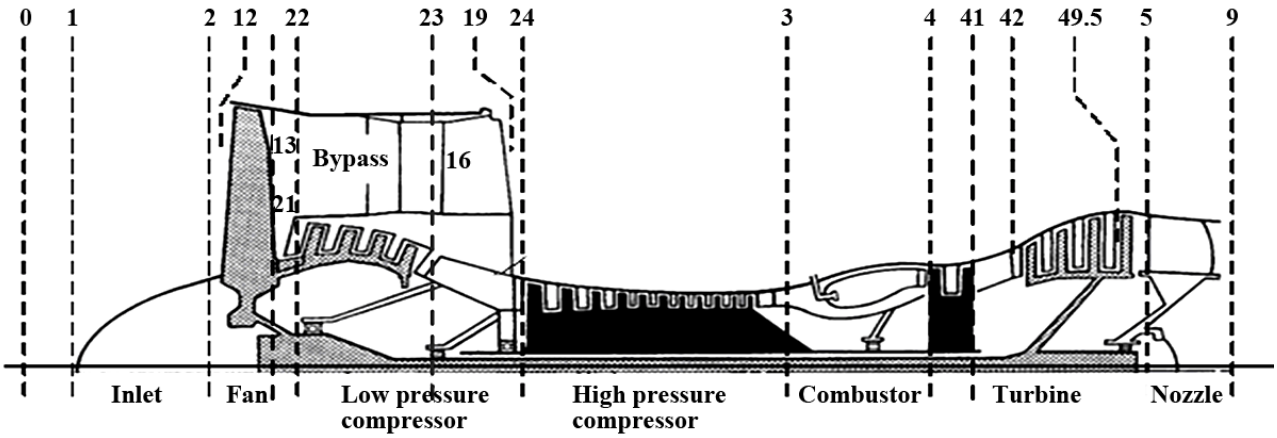

A turbofan engine mathematical model discussed in the paper consists of a number of individual components, each of which requires a number of input variables and generates one or more variables, denoted as Component Level Model (CLM). The model contains mathematical equations, maps, tables, *etc.*, which describe the thermodynamic relationships between various variables in the engine. In the CLM, we assume combustion delay is neglected; the component characteristics are unchanged with the Reynolds number, and zero-dimension flow. The thermodynamic parameters in cross sections of each component, such as the total temperature, total pressure, flow capacity, and efficiency, can be calculated as in references [46–48]. The common operation of a turbofan engine in steady state follows flow capacity balance and power balance, and which are separated expressed as follows:

$$\begin{cases} W_{22} - W_{21} = 0 \\ W_{24} - W_{23} = 0 \\ W_{41} - W_{HTcool1} - W_{HTcool2} - W_4 = 0 \\ W_{42} - W_{41} = 0 \\ W_9 - W_5 = 0 \\ W_{19} - W_{16} = 0 \end{cases} \tag{17}$$

$$\begin{cases} N_{HT}\eta_{Hspool} - N_C - N_T = 0 \\ N_{LT}\eta_{Lspool} - N_F - N_B = 0 \end{cases} \tag{18}$$

where W_{21} is the fan core duct outlet flow capacity, W_{22} the booster inlet one, W_{23} the booster outlet one, W_{24} the high pressure compressor (HPC) inlet one, W_4 the combustor outlet one, W_{41} the high pressure turbine (HPT) outlet one, W_{42} the low pressure turbine (LPT) inlet one, W_5 the LPT outlet one, W_9 the nozzle core duct outlet one, W_{16} the fan bypass duct outlet one, W_{19} the bypass duct outlet

one. Four cooling air streams $W_{HTcool1}$, $W_{HTcool2}$, $W_{LTcool1}$, $W_{LTcool2}$ from the HPC are separately drawn in to cool the turbine inlet guide vane, blade-tip of the HPT and the LPT. N_{HT} and N_{LT} are the power produced by the HPT and LPT, N_C, N_T, N_F, and N_B are the power used for the HPC, accessories, fan, and booster, η_{Hspool} and η_{Lspool} are the high pressure spool efficiency and the low pressure spool efficiency, respectively.

The CLM in steady state has eight balance equations, seen in Equations (17) and (18), therefore, there are eight guess variables used to determine the engine steady operating condition, which are low pressure spool speed n_L, high pressure spool speed n_H, fan blade tip pressure ratio π_{Ft}, fan blade root pressure ratio π_{Fr}, booster pressure ratio π_B, compressor pressure ratio π_C, HPT pressure ratio π_{HT}, and LPT pressure ratio π_{LT}. The common operating expressions of the CLM in steady state can be denoted as the following nonlinear equations:

$$f_j(n_L, n_H, \pi_{Ft}, \pi_{Fr}, \pi_B, \pi_C, \pi_{HT}, \pi_{LT}) = 0, \qquad j = 1, 2, \ldots, 8 \tag{19}$$

The common operating expressions of the turbofan engine in dynamics follows the flow capacity balance as same as the steady state ones in Equation (17). However, the two spools powers in dynamics are no longer balanced as in Equation (18), so they are replaced by the following equations defining the rotor dynamics:

$$\begin{cases} \left(\dfrac{30}{\pi}\right)^2 \dfrac{1}{J_H n_H}\left[N_{HT}\eta_{Hspool} - N_C - N_T\right] = \dfrac{dn_H}{dt} \\ \left(\dfrac{30}{\pi}\right)^2 \dfrac{1}{J_L n_L}\left[N_{LT}\eta_{Lspool} - N_F - N_B\right] = \dfrac{dn_L}{dt} \end{cases} \tag{20}$$

where J_H, and J_L are the rotor inertias of the high pressure spool and low pressure spool. There are six guess variables, $\pi_{Ft}, \pi_{Fr}, \pi_B, \pi_C, \pi_{HT}, \pi_{LT}$, for the CLM in dynamics, and the current spool speeds are calculated via the speeds in the last step and the accelerations from Equation (20):

$$f_j(\pi_{Ft}, \pi_{Fr}, \pi_B, \pi_C, \pi_{HT}, \pi_{LT}) = 0, \qquad j = 1, 2, \ldots, 6 \tag{21}$$

The nonlinear expressions both in steady state, Equation (19), and dynamics, Equation (21), are solved via Newton-Raphson approach. Iterative solution of nonlinear equations each step stops once one of the following conditions is satisfied: the maximum iteration number equals 10, or the iteration error is less than 0.01. The core rotating component efficiency/flow capacity is usually used to represent the aircraft engine gas path performance, seen in Table 2, the degradations of which are denoted as health parameters as follows:

$$\begin{aligned} \Delta SE_i &= \frac{SE_i}{SE_{i,r}} - 1 \qquad i = 1, 2, 3, 4 \\ \Delta SW_j &= \frac{SW_j}{SW_{j,r}} - 1 \qquad j = 1, 2, 3 \end{aligned} \tag{22}$$

The health parameters and health parameter degradations are modeled in the CLM for the problem studied in the paper. The CLM is written using C language and packaged with dynamic link library (DLL) for use in the Matlab environment [47,49]. The outputs of function in DLL are the

measurements, shown in Table 3, and the inputs consist of height, Mach number, Wf , A_8, health parameters, and the noise. The CLM balances flow capacity (power) equations of the system is at a rate of 200 Hz, and the sampling frequency used for the nonlinear model health monitoring is 50 Hz. The discretized time invariant equations that model the turbofan engine from the dynamic CLM can be summarized as follows:

$$x_{aug,k+1} = \begin{pmatrix} x_{k+1} \\ \Delta h_{k+1} \end{pmatrix} = \begin{pmatrix} f(x_k, \Delta h_k, u_k, c_{ond}) \\ \Delta h_k \end{pmatrix} + \begin{pmatrix} w_{x,k} \\ w_{p,k} \end{pmatrix}$$
$$y_k = h(x_k, \Delta h_k, u_k) + v_k \tag{23}$$

where u is the 2-element control vector, $x = [n_L, n_H]$ the 2-element state vector, $\Delta h = [\Delta SE_1, \Delta SW_1, \Delta SE_2, \Delta SW_2, \Delta SE_3, \Delta SW_3, \Delta SE_4]^T$ the 7-element performance vector, c_{ond} the 2-element environmental vector, and y the 9-element measurement vector [29,46]. The rapid degeneration and the gradual degeneration to the components are separately injected over time. Between measurement times their deviations can be approximated by the zero mean noise $w_{h,k}$, and v_k represents measurement noise. Nonlinear filtering approaches can be used with (23) to estimate the augment state vector $x_{aug,k}$.

The controls, health parameters, and measurements are summarized in Tables 1–3, along with their values at the design operating point considered in this paper, which is at sea level static conditions ($H = 0$ km, $Ma = 0$). Table 3 also shows typical standard deviations for the measurements, based on experience, which are both used in the CLM and the estimators to build up the measurement noise covariance. Sensor dynamics are assumed to be high enough bandwidth that they can be ignored in the dynamic equations.

Table 1. CLM turbofan model controls and nominal values.

Control	Acronyms	Nominal values
Fuel flow	Wf	2.5 kg/s
Variable nozzle aera	A_8	0.54 m^2

Table 2. CLM turbofan model health parameter, nominal value, standard deviation and degeneration maximum.

Augment state	Acronyms	Nominal value	Standard deviation	Deteriorate maximum (%)
Fan airflow capacity	SW_1	1	0.0005	−3.65
Fan efficiency	SE_1	1	0.0005	−2.85
HPC airflow capacity	SW_2	1	0.0005	−14.1
HPC efficiency	SE_2	1	0.0005	−9.4
HPT airflow capacity	SW_3	1	0.0005	2.57
HPT efficiency	SE_3	1	0.0005	−3.81
LPT efficiency	SW_4	1	0.0005	−1.08

Table 3. CLM turbofan model measurements, nominal values, and standard deviation.

Measurement	Acronyms	Nominal values	Standard deviation
Low pressure spool speed	n_L	3771 RPM	0.0015
High pressure spool speed	n_H	10241 RPM	0.0015
Fan exit pressure	P_{13}	172253 Pa	0.0015
HPC inlet temperature	T_{24}	707 K	0.002
HPC inlet pressure	P_{24}	344505 Pa	0.0015
HPC exit temperature	T_3	1078 K	0.002
HPC exit pressure	P_3	2940997 Pa	0.0015
LPT exit temperature	T_5	1086 K	0.002
LPT exit pressure	P_5	159367 Pa	0.0015

4. Simulations and Analysis

In this section, the nonlinear filtering approaches discussed in this paper, and used for gas path performance estimation, are validated using Matlab. The normal operating parameters of the turbofan engine are depicted in Tables 1 and 3. Gaussian noise whose magnitude is specified in Table 3 is added to the clean simulated measurements to make them representative of real data. Two types process noise with the same covariance in Table 2, Gaussian distribution and Rayleigh distribution, are separately introduced to build up the Gaussian system and the non-Gaussian one. The PDF of Rayleigh distribution is as follows:

$$f(x)=\begin{cases}\dfrac{x}{\sigma^2}\exp\left(\dfrac{-x^2}{2\sigma^2}\right) & x>0\\ 0 & x\le 0\end{cases} \tag{24}$$

The mean and covariance of Rayleigh distribution are separately $\sigma\sqrt{\frac{\pi}{2}},\frac{4-\pi}{2}\sigma^2$, and this type process noise introduced into the system is a non-zero mean. In order to avoid health parameter degeneration estimates influenced by the non-zero mean process noise, the PDF of Rayleigh distribution is moved left with $\sigma\sqrt{\frac{\pi}{2}}$.

The engine's health parameters are initialized to the values shown in Table 2. Considering foreign-object damage to the engine, rapid degradations are carried out. The following rapid faults are simulated at 1 second: (1) −9% on SE2, (2) −3% on SE1, −9% on SE2, and 3% on SW3, which are labeled fault 1 and fault 2, respectively. Engine wear due to normal operation, gradual degeneration, is also simulated by linearly drifting values of nearly all health parameters, starting from 1 and with the maximum degradation in Table 2 at the end of the sequence. Both in the PF and the constrained EKPF (cEKPF) framework, the number of particles is 50. The constraint value of each health parameter is set to more than 10% of its deteriorate maximum.

4.1. Rapid Deterioration Simulations

Rapid faults simulations with the three algorithms namely the EKF tool, the PF tool, and the cEKPF tool—are presented and discussed. Figure 3 depicts the health parameters estimation, in the case

of −9% on SE2 at 1s, with the three tools in the Gaussian system. As can be seen from Figure 4, three health parameters separately track the performance shifts well in the Gaussian system under the Fault 2 conditions.

Figure 3. Health parameters estimation with Gaussian noise under the Fault 1. (**a**) The EKF; (**b**) the PF; (**c**) the cEKPF.

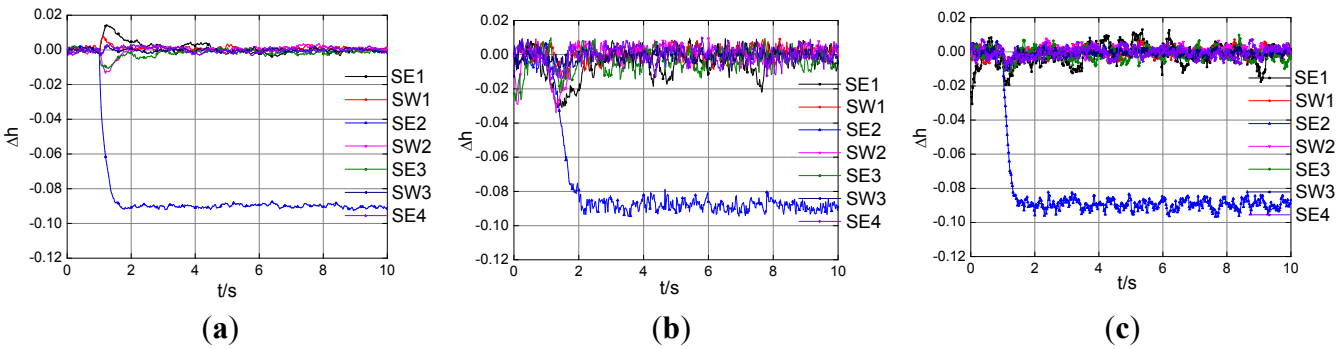

Figure 4. Health parameters estimation with Gaussian noise under the Fault 2. (**a**) the EKF; (**b**) the PF; (**c**) the cEKPF.

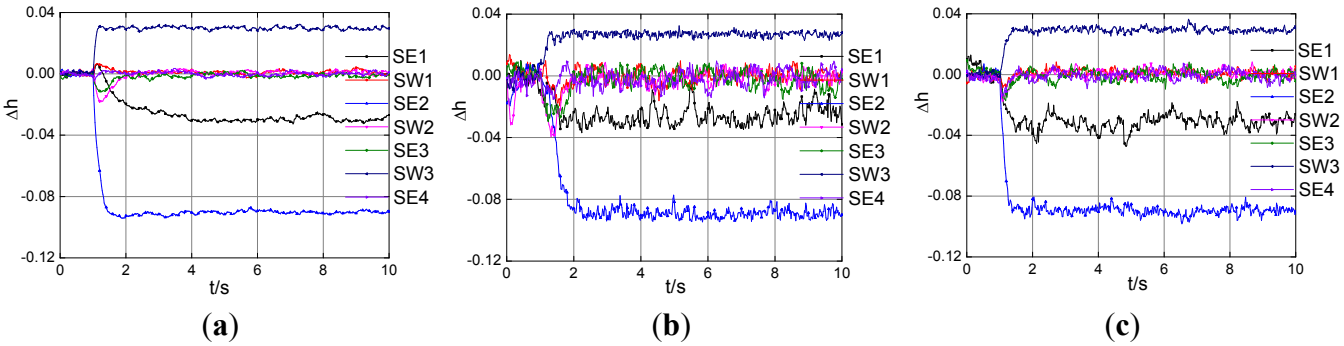

In order to compare the EKF, the PF, and the cEKPF more rationally, the process noise covariance matrices Q and measurement noise covariance matrices R are the same in three algorithms, respectively. The quality of the estimation performed by the three tools is assessed in terms of the estimation mean error (ME) and its standard deviation (SD) over the last 2 s of the sequence (100 samples):

$$ME(m) = \left(\frac{1}{D_e - D_s + 1} \sum_{k=D_s}^{D_e} \hat{h}_k(m) \right) - h(m)$$
$$SD(m) = \sqrt{\frac{1}{D_e - D_s} \sum_{k=D_s}^{D_e} \left(\hat{h}_k(m) - \frac{1}{D_e - D_s + 1} \sum_{k=D_s}^{D_e} \hat{h}_k(m) \right)} \tag{25}$$

where $h(m)$ is the true magnitude of deterioration of the mth element of the health parameters, and $D_s = 401,\ D_e = 500$.

Table 4 reports the figure of merit defined by Equation (25) for the different fault-case with Gaussian noise that have been considered in the present study. For the rapid deterioration of Fault 1 and Fault 2, both the EKF and cEKPF perform a better accurate tracking of the engine conditions than the PF, which is confirmed by their estimation mean errors in Table 4. The health parameters estimated

with the PF jump seriously in Figure 3(b) and Figure 4(b), and its standard deviations are almost the biggest one compared to other two tools, as seen from the Table 4. Bold numerical values correspond to the statistical characteristics of the degraded health parameters.

Table 4. Mean error and standard deviation of the estimation with Gaussian noise.

		Fault 1			Fault 2		
		EKF	**PF**	**cEKPF**	**EKF**	**PF**	**cEKPF**
ME (10^{-4})	SE1	−4.42	52.53	0.55	2.89	3.03	−2.88
	SW1	8.47	7.52	0.75	8.12	16.38	8.97
	SE2	0.08	−3.29	4.27	−1.28	−1.95	1.81
	SW2	7.74	5.54	4.79	8.20	12.25	11.49
	SE3	−11.22	−34.73	−14.07	−8.56	7.71	−8.23
	SW3	−2.17	−4.04	−5.28	−2.51	−5.27	−5.26
	SE4	−3.08	17.28	−4.49	−3.02	−24.76	−4.98
SD (10^{-3})	SE1	1.65	9.54	5.52	1.46	12.63	4.69
	SW1	0.89	4.39	2.41	1.27	4.36	2.18
	SE2	0.96	4.41	2.86	0.88	5.54	2.70
	SW2	1.05	4.19	2.04	1.03	5.24	2.39
	SE3	0.96	6.28	3.07	1.13	7.25	3.25
	SW3	0.81	2.60	1.55	0.97	3.26	1.61
	SE4	1.11	5.01	2.96	1.14	5.31	2.91

Figure 5 show the health parameters estimation, in the case of −9% on SE2 at 1 s, with the three tools in the nonlinear Gaussian system. We can see from the Figure 5(a) that the health parameters SE1 and SE2 shift to 5% and −10% at nearly 2 s and then drift away, while the remaining health parameter delta values drift from zero. The estimated health parameter SE2 delta is about −9%, and the others about the zero, as shown in Figure 5(b) and Figure 5(c). Therefore, both the PF and the cEKPF can represent the engine conditions well, while the EKF produces misdiagnostics in the non-Gaussian system under the Fault 1 conditions. In Figure 6, the three degraded health parameters are tracked well both with the PF and the cEKPF, except the EKF.

Figure 5. Health parameters estimation with non-Gaussian process noise under the Fault 1. (**a**) The EKF; (**b**) the PF; (**c**) the cEKPF.

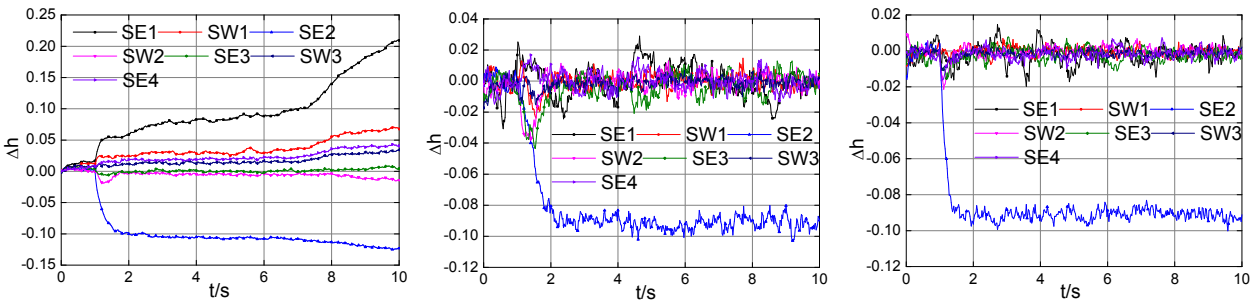

(**a**) (**b**) (**c**)

Figure 6. Health parameters estimation with non-Gaussian process noise under the Fault 2. (**a**) The EKF; (**b**) the PF; (**c**) the cEKPF.

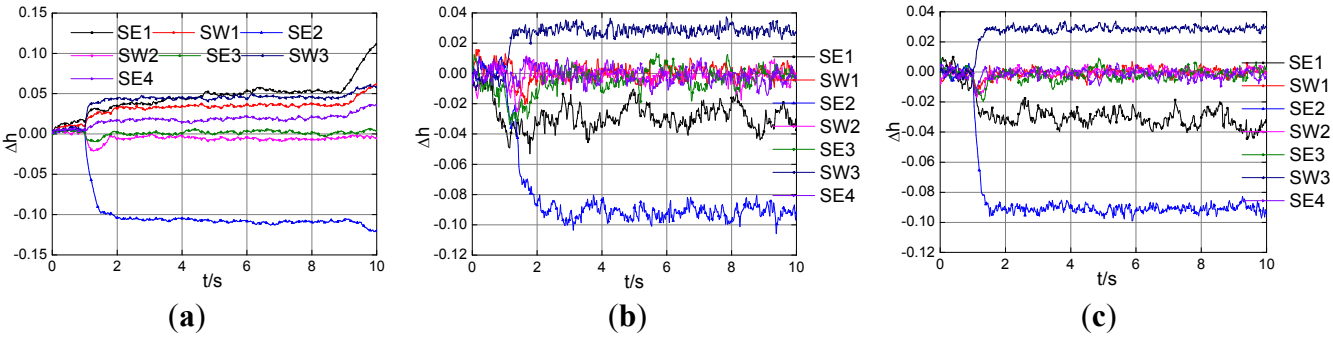

Table 5 presents mean error and standard deviation of the estimation defined by Equation (25) for the Fault 1 and the Fault 2 in the non-Gaussian system. For the rapid deterioration of the two fault modes with the non-Gaussian process noise, the cEKPF performs the most accurate estimation, then the PF, while the EKF fails in the estimation. It is confirmed by their estimation mean errors and standard deviations, especially the degraded health parameters that are indicated in bold in Table 5.

Table 5. Mean error and standard deviation of the estimation with non-Gaussian noise.

		Fault 1			Fault 2		
		EKF	**PF**	**cEKPF**	**EKF**	**PF**	**cEKPF**
ME (10^{-3})	SE1	122.72	1.32	−1.01	86.97	2.23	−1.62
	SW1	43.90	−0.11	−0.43	37.75	0.44	0.11
	SE2	−21.78	−1.95	−0.82	−19.28	−1.68	−1.16
	SW2	−6.84	0.04	0.07	−5.57	−1.66	0.03
	SE3	16.68	−2.44	−2.30	2.34	−2.10	−1.16
	SW3	20.32	−0.42	−1.41	16.99	−1.29	−1.23
	SE4	28.04	0.45	−1.46	20.85	−1.91	−1.74
SD (10^{-2})	SE1	4.32	0.97	0.60	1.52	0.67	0.53
	SW1	1.50	0.45	0.20	0.63	0.39	0.24
	SE2	0.61	0.42	0.28	0.31	0.41	0.25
	SW2	0.30	0.44	0.24	0.17	0.39	0.22
	SE3	0.25	0.70	0.32	0.20	0.60	0.31
	SW3	0.71	0.28	0.16	0.43	0.28	0.15
	SE4	0.85	0.57	0.30	0.51	0.48	0.29

4.2. Gradual Degeneration Simulation

Gradual degeneration of a turbofan engine is simulated by linearly drifting values of nearly all health parameters, starting from their nominal values and with the following degradation at the end of the sequence (6,000 cycle number): −2.85% on SE1, −3.65% on SW1, −9.4% on SE2, −14.1% on SW2, −3.81% on SE3, 2.57% on SW3, −1.08% on SE4. There are 21 steady operating points in the whole degradation range. Figure 7 and Figure 8 separately show the estimation performance of the three nonlinear filtering methods under the gradual degradation with Gaussian noise and non-Gaussian noise.

The health parameter degeneration value in the Gaussian system can be estimated with the EKF, the PF, and the cEKPF, while the PF performs less accurate tracking than the others, as shown in Figure 7. When the Rayleigh distribution noise is introduced to the model, the estimation performance with the EKF is obviously decreased compared with Figure 7(a) and Figure 8(a). Table 6 shows the estimation error square sum of 21 steady operating points in the whole degenerate range. In Table 6 we can see that the performance of the PF and the cEKPF will not be much change with the various process noise.

Figure 7. Health parameters estimation with Gaussian noise under the gradual degradation. (**a**) The EKF; (**b**) the PF; (**c**) the cEKPF.

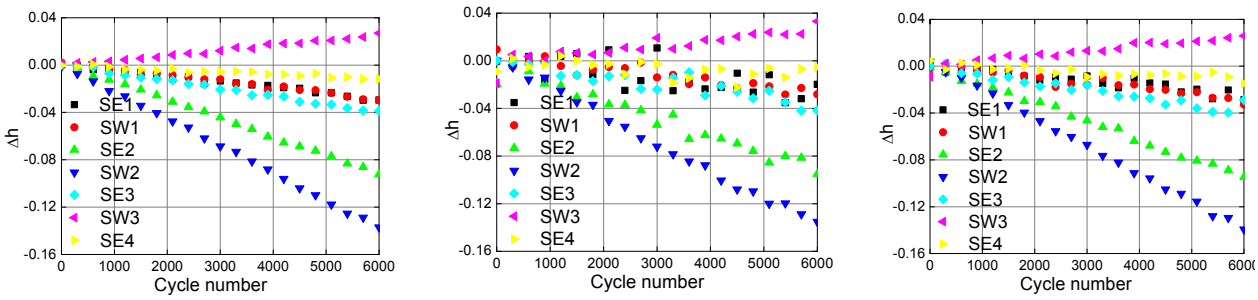

(**a**) (**b**) (**c**)

Figure 8. Health parameters estimation with non-Gaussian noise under the gradual degradation. (**a**) The EKF; (**b**) the PF; (**c**) the cEKPF.

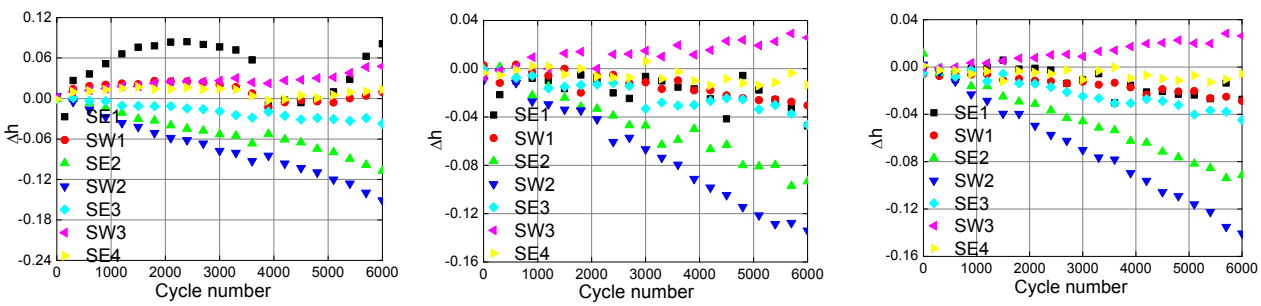

(**a**) (**b**) (**c**)

Table 6. Estimation error square sum at the steady state (10^{-2}).

	EKF	PF	cEKPF
Gaussian system	6.74	7.61	6.85
Non-Gaussian system	21.66	8.19	6.93

4.3. Computational Load

A computational load analysis was performed using simple Matlab profiling tools. Specifically, a unit-less computation load factor was determined by normalizing the Matlab m-file run time with the duration of operating data filtered. The computational time average of 20 tests is calculated, and the results are summarized in Table 7.

Table 7. Computational effort of the EKF, the PF, and the cEKPF.

	System with Gaussian noise		System with non-Gaussian noise	
	Fault 1	Fault 2	Fault 1	Fault 2
EKF	7.7	7.7	7.8	8.3
PF	27	26.7	29	30.3
cEKPF	23	21.8	27.2	26

As indicated, the EKF requires a significantly less load than both the PF and cEKPF no matter whether Gaussian noise is injected into the system, although it performs poorly tracking the engine conditions in the non-Gaussian system. The PF and cEKPF load are heavily dependent on the number of particles used, however, the cEKPF consumes less time for estimation compared to the PF.

4.4. Potential Effect

The turbofan engine gas path health parameters are estimated by nonlinear filter approaches with all nine measurements in Table 3 in the simulation above. While the number of available sensors for gas path analysis might decrease in practice, *i.e.* one sensor failure. The following experiments that health parameters are estimated with eight measurements are carried out, and used to make comparisons of the EKPF and the cEKPF. Figure 9 show that the health parameter estimates, in the case of Fault 1, with all measurements except the sensor *P5* in the Gaussian system by the EKPF and the cEKPF. As can be seen from Figure 9(a), the estimate of *SE2* decreases to about −0.09 before 2s, and other health parameters are nearly unchanged, which are consistent with the Fault 1. However, in Figure 9(b) there are three health parameter estimates, *SE2*, *SE3*, and *SE4*, drifting from zero after 1s, false estimates are done via the EKPF.

Figure 9. Health parameters estimation with all measurements except *P5* in Gaussian system under the Fault 1. (**a**) The cEKPF; (**b**) the EKPF.

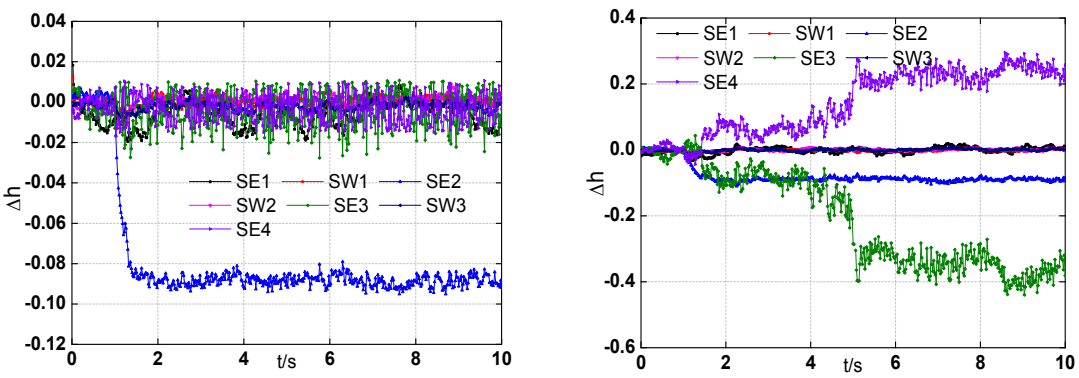

(**a**) (**b**)

Table 8 represents the mean error sum of the health parameter estimates, $SME = \sum_{m=1}^{7} ME(m)$, with all measurements except one sensor in turn in the Gaussian system. We can see that the health parameter estimations can't be implemented via the EKPF under three conditions of sensor selection: all measurements except n_L, except P_{13}, or except T_{24}, respectively. Although the estimates are convergent and the *MSE* can be calculated by the EKPF under the remaining six sensor selected

condition, the *MSE* are much bigger than that by the cEKPF. Therefore, compared to the EKPF, the cEKPF is an effective estimator and can be still used for gas path health monitoring with one less sensor.

Table 8. Estimation error square sum with the eight measurements in Gaussian system.

	n_L	n_H	P_{13}	T_{24}	P_{24}	T_3	P_3	T_5	P_5
EKPF	x	0.875	x	x	1.001	0.632	0.284	1.552	0.909
cEKPF	0.276	0.207	0.188	0.195	0.193	0.187	0.191	0.198	0.196

The particle number is an important parameter in variants of the PF algorithm, and the estimate accuracy and computational load rest with the particle scale. Table 9 shows the comparisons of estimate performance with nine measurements by the cEKPF under three particle scales: $N = 30$, $N = 50$, and $N = 100$. We can make some interesting observations from the Table 9, the *SME* decrease and the computational load steadily increase as the particle number increases from 30 to 100 both under Fault 1 and Fault 2. Compared to the particle number increase from 30 to 50, there does not appear to be evidently any improvement in the estimation accuracy when the number goes from 50 to 100. The particle number equal to 50 is reasonable in this case for gas path health monitoring.

Table 9. Comparisons of estimate performance by the cEKPF under different particle scales.

	Fault 1			**Fault 2**		
	$N = 30$	$N = 50$	$N = 100$	$N = 30$	$N = 50$	$N = 100$
$SME(10^{-2})$	0.366	0.343	0.342	0.472	0.438	0.432
Time(s)	14.1	23	40.8	14.1	21.9	40.3

5. Conclusions and Future Work

Within this study, a widely used nonlinear estimation method, the particle filter based on Monte Carlo sampling algorithms, is implemented for gas path performance monitoring for turbofan engines. Because of particle degeneracy in the generic PF framework, the EKF is introduced to use the latest observation value to amend the state transition model of particles and its amount of calculation is not big. Considering the degradation magnitude of health parameters is within a certain range during the on-wing cycle, the constrained strategy of particle update is designed and combined with the EKPF, and then the detailed constrained EKPF is proposed and presented.

This paper has compared the three nonlinear filters based estimation approaches, the EKF, the PF, and the constrained EKPF, for the evaluation of turbofan engine gas path health. The health monitoring system with Gaussian noise and non-Gaussian noise (Rayleigh distribution process noise), keeping the same process noise variances, are set up separately. The accuracy and computational load under the different cases of abrupt faults and gradual degradation are used to evaluate the three filtering methods. Compared to the EKF, the PF and the cEKPF perform with more adaptability to the non-Gaussian system. According to the experiments on health parameter estimates with less measurements, we can see that the effect of cEKPF is obviously much better than that of the EKPF. The particle number influenced to the estimate accuracy and computational effort is discussed in the cEKPF, and the better

particle scale for gas path health monitoring is selected. The improvements brought by the EKF with constrained mechanism to a generic PF have enhanced the computational effort of the PF algorithm.

In summary, the proposed cEKPF is an effective way to estimate health condition for complicated machines with undetermined noise. The non-Gaussian system is defined as the system with the Rayleigh distribution process noise in present paper, while the non-normal distribution process noise, the non-normal distribution measurement noise, or both of them introduced to the system will produce the non-Gaussian system. Therefore, it would be interesting to see how the conclusions of this paper might change with the other forms of non-Gaussian system.

Acknowledgments

This work has been supported by the Fundamental Research Funds for the Central Universities (No. NZ2012110), and the National Nature Science Foundation of China (No. 51276087).

References

1. Simon, D.L. *An Integrated Architecture for On-Board Aircraft: Engine Performance Trend Monitoring and Gas Path Fault Diagnostics*; Technical Report for National Aeronautics and Space Administration: Cleveland, OH, USA, 2010.
2. Kurz, R.; Brun, K. Degradation in gas turbine systems. *J. Eng. Gas Turbines Power* **2001**, *123*, 70–77.
3. James, A.T.; Litt, J.S. A foreign object damage event detector data fusion system for turbofan engines. *J. Aerosp. Comput. Inf. Commun*. **2004**, *2*, 291–308.
4. Tang, L.; Decastro, J.A.; Zhang, X.; Ramos, L.F.; Simon, D.L. A Unified Nonlinear Adaptive Approach for Detection and Isolation of Engine Faults. In *Proceedings of the Turbo Expo 2010: Power for Land, Sea and Air*, Glasgow, UK, 14–18 June 2010; pp. 143–153.
5. Garg, S. *Propulsion Controls and Diagnostics Research at NASA Glenn Research Center*; Technical Report for National Aeronautics and Space Administration: Cleveland, OH, USA, 2010.
6. Su, W.; Zhao, Y.; Sun, J. Novel weighted least squares support vector regression for thrust estimation on performance deterioration of aero-engine. *Trans. Nanjing Univ. Aeronaut. Astronaut*. **2012**, *29*, 25–32.
7. Luppold, R.H.; Roman, J.R.; Gallops, G.W.; Keer, L.J. Estimating in-Flight Engine Performance Variations Using Kalman Filter Concepts. In *Proceedings of the 25th AIAA/ASME/SAE/ASEE Joint Propulsion Conference*, Monterey, CA, USA, 10–12 July 1989.
8. Doel, D. An assessment of weighted-least-squares-based gas path analysis. *J. Eng. Gas Turbines Power* **1994**, *116*, 366–373.
9. DePold, H.; Gass, F. The application of expert systems and neural networks to gas turbine prognostics and diagnostics. *J. Eng. Gas Turbines Power* **1999**, *121*, 607–612.
10. Joly, R.B.; Ogaji, S.O. T.; Singh, R.; Probert, S.D. Gas-turbine diagnostics using artificial neural-networks for a high bypass ratio military turbofan engine. *Appl. Energy* **2004**, *78*, 397–418.
11. Kobayashi, T.; Simon, D.L. A Hybrid Neural Network-Genetic Algorithm Technique for Aircraft Engine Performance Diagnostics. In *Proceedings of the 37th AIAA/ASME/SAE/ASEE Joint Propulsion Conference*, Salt Lake City, UT, USA, 8–11 July 2001.

12. Ogaji, S.O.T.; Marinai, S.; Sampath, S.; Singh, R.; Prober, S.D. Gas-turbine fault diagnostics: a fuzzy-logic approach. *Appl. Energy* **2005**, *82*, 81–89.
13. Volponi, A.; DePold, H.; Ganguli, R.; Daguang, C. The use of Kalman filter and neural network methodologies in gas turbine performance diagnostics: a comparative study. *J. Eng. Gas Turbines Power* **2003**, *125*, 917–924.
14. Domogianopoulos, D.; Hios, J.; Fassois, S. Aircraft engine health management via stochastic modeling of flight data interrelations. *Aerosp. Sci. Technol*. **2011**, *16*, 70–81.
15. Li, Y.G.; Korakianitis, T. Nonlinear weighted-least-squares estimation approach for gas-turbine diagnostic applications. *J. Propuls. Power* **2011**, *27*, 337–345.
16. Li, Y.G.; Ghafir, M.F. A.; Wang, L.; Singh, R.; Huang, K.; Feng, X.; Zhang, W. Improved multiple point nonlinear genetic algorithm based performance adaptation using least square method. *J. Eng. Gas Turbines Power* **2012**, *134*, 49–60.
17. Li, Y.G.; Pilidis, P. GA-based design-point performance adaptation and its comparison with ICM-based approach GA-based design-point performance adaptation and its comparison with ICM-based approach. *Appl. Energy* **2010**, *87*, 340–348.
18. Brotherton, T.; Volponi, A.; Luppold, R.; Simon, D.L. eSTORM: Enhanced Self Tuning on-board Real-Time Engine Model. In *Proceedings of the 2003 IEEE Aerospace Conference*, Big Sky, MT, USA, 8–15 March 2003; pp. 3075–3086.
19. Volponi, A. *Enhanced Self Tuning On-Board Real-Time Model (eSTORM) for Aircraft Engine Performance Health Tracking*; Technical Report for Pratt and Whitney Aircraft Group: East Hartford, CT, USA, 2008.
20. Simon, D.; Simon, D.L. *Kalman Filter Constraint Tuning for Turbofan Engine Health Estimation*; Technical Report for National Aeronautics and Space Administration: Cleveland, OH, USA, 2005.
21. Simon, D.; Simon, D.L. Constrained Kalman filtering via density function truncation for turbofan engine health estimation. *Int. J. Syst. Sci.* **2010**, *41*, 159–171.
22. Litt, J.S.; Simon, D.L. *Toward a Real-Time Measurement-Based System for Estimation of Helicopter Engine Degradation due to Compressor Erosion*; Technical Report for National Aeronautics and Space Administration: Cleveland, OH, USA, 2007.
23. Simon, D.L.; Garg, S. *A Systematic Approach to Sensor Selection for Aircraft Engine Health Estimation*; Technical Report for National Aeronautics and Space Administration: Cleveland, OH, USA, 2009.
24. Simon, D.L.; Armstrong, J.B.; Garg, S. *Application of an Optimal Tuner Selection Approach for On-Board Self-Tuning Engine Models*; Technical Report for National Aeronautics and Space Administration: Cleveland, OH, USA, 2012.
25. Kobayashi, T.; Simon, D.L.; Litt, J.S. Application of a Constant Gain Extended Kalman Filter for In-Flight Estimation of Aircraft Engine Performance Parameters. In *Proceedings of ASME Turbo Expo 2005: Power for Land, Sea, and Air*, Reno, NV, USA, 6–9 June 2005; pp. 617–628.
26. Kobayashi, T.; Simon, D.L. Aircraft Engine On-Line Diagnostics Through Dual-Channel Sensor Measurements: Development of a Baseline System. In *Proceedings of ASME Turbo Expo 2008: Power for Land, Sea, and Air*, Berlin, Germany, 9–13 June 2008; pp. 77–89.
27. Borguet, S.; Leonard, O. Comparison of adaptive filters for gas turbine performance monitoring. *J. Comput. Appl. Math.* **2010**, *234*, 2202–2212.

28. Naderi, E.; Meskin, N.; Khorasani, K. Nonlinear fault diagnosis of jet engines by using a multiple model-based approach. *J. Eng. Gas Turbines Power* **2012**, *134*, 011602: 1–011602: 10.
29. Simon, D. A comparison of filtering approaches for aircraft engine health estimation. *Aerosp. Sci. Technol.* **2008**, *12*, 276–284.
30. Gordon, N.; Salmond, D.; Smith, A. Novel Approach to Nonlinear/Non-Gaussian Bayesian State Estimation. *Radar Signal Process. IEE Proc. F* **1993**, *140*, 107–113.
31. Doucet, A.; Godsill, S. *On Sequential Simulation-Based Methods for Bayesian Filtering*; Technical Report; Department of Engineering, Cambridge University: Cambridge, UK, 1998.
32. Freitas, N.; Doucet, A.; Gordon, N. *Sequential Monte Carlo Methods in Practice*; Springer: New York, NY, USA, 2001.
33. Doucet, A.; Godsill, S.; Andrieu, C. On sequential Monte Carlo sampling methods for Bayesian filtering. *Stat. Comput.* **2000**, *10*, 197–208.
34. Boloc, M.; Djuric, P.; Hong, S. Resampling algorithms for particle filters: a computational complexity perspective. *EURASIP J. Appl. Signal Process*. **2004**, *15*, 2267–2277.
35. Orchard, M.E.; Vachtsevanos, G.J. A Particle Filtering-Based Framework for Real-Time Fault Diagnosis and Failure Prognosis in a Turbine Engine. In *Proceedings of Mediterranean Conference on Control and Automation*, Athens, Greece, 27–29 July 2007.
36. Li, B.; Liu, Z.; Li, X. Research of UAV Engine Fault Prediction Based on Particle Filter. In *Proceedings of the 9th International Conference on Electronic Measurement & Instruments*, Beijing, China, 16–19 August 2009.
37. Rigatos, G.G. Nonlinear Kalman filters ANS particle filters for integrated navigation of unmanned aerial Vehicles. *Robot. Auton. Syst.* **2012**, *60*, 978–995.
38. Gross, J.; Gu, Y.; Gururajan, S.; Seanor, B. Napolitano, M.R. A Comparison of Extended Kalman Filter, Sigma-Point Kalman Filter, and Particle Filter in GPS/INS Sensor Fusion. In *Proceedings of AIAA Guidance*, *Navigation*, *and Control Conference*, Toronto, Canada, 2–5 August 2010.
39. Freitas, J.F.; Niranjan, M.; Gee, A.H.; Doucet, A. Sequential Monte Carlo methods to train neural network models. *Neural Comput.* **2000**, *12*, 955–993.
40. Demirbas, K. A novel real-time adaptive suboptimal recursive state estimation scheme for nonlinear discrete dynamic systems with non-Gaussian noise. *Digit. Signal Process*. **2012**, *22*, 593–604.
41. Hou, S.Y.; Hung, H.S.; Chang, S.H.; Liu, J.C. Novel algorithms for tracking multiple targets. *J. Mar. Sci. Technol.* **2010**, *18*, 259–267.
42. Andreas, G.; Andrea, W. *Evaluating Derivatives: Principles and Techniques of Algorithmic Differentiation*, 2nd ed.; Society for Industrial and Applied Mathematics: Philadelphia, PA, USA, 2008.
43. Shao, X.; Huang, B.; Lee, J.M. Constrained Bayesian state estimation- A comparative study and a new particle filter based approach. *J. Process Control* **2010**, *20*, 143–157.
44. Kyriakides, K.; Morrell, D.; Supplppola, A.P. A Particle Filtering Approach to Constrained Motion Estimation in Tracking Multiple Targets. In *Proceedings of the 39th Asilomar Conference on Signals*, *Systems and Computer*, Pacific Grove, CA, USA, 30 October–2 November 2005.
45. Lang, L.; Chen, W.; Bakshi, B.; Goel, P.; Ungarala, S. Bayesian estimation via sequential Monte Carlo sampling-constrained dynamic systems. *Automatica* **2007**, *43*, 1615–1622.

46. Sun, J.G.; Vasilyev, V.; Ilyasov, B. *Advanced Multivariable Control Systems of Aeroengines*; Beijing University of Aeronautics & Astronautics: Beijing, China, 2005.
47. Zhou, W.X. Research on Object-Oriented Modeling and Simulation for Aeroengine and Control System. Ph.D. Thesis, Nanjing University of Aeronautics and Astronautics, Nanjing, China, 2006.
48. *The Research and Technology Organization of NATO, Performance Prediction and Simulation of Gas Turbine Engine Operation for Aircraft, Marine, Vehicular, and Power Generation*; NATO Research and Technology Organization: Neuilly-Sur-Seine, France, 2007.
49. Lu, F.; Huang, J. Engine component performance prognostics based on decision fusion. *Acta Aeronautica et Astronautica Sinica* **2009**, *30*, 1795–1800.